Synchrotron-Based Techniques Shed Light on Mechanisms of Plant Sensitivity and Tolerance to High Manganese in the Root Environment[1][OPEN]

F. Pax C. Blamey, Maria C. Hernandez-Soriano, Miaomiao Cheng, Caixian Tang, David J. Paterson, Enzo Lombi, Wei Hong Wang, Kirk G. Scheckel, and Peter M. Kopittke*

School of Agriculture and Food Sciences, The University of Queensland, St. Lucia, Queensland 4072, Australia (F.P.C.B., M.C.H.-S., P.M.K.); Centre for AgriBioscience, La Trobe University, Bundoora, Victoria 3086, Australia (M.C., C.T.); Australian Synchrotron, Clayton, Victoria 3168, Australia (D.J.P.); Centre for Environmental Risk Assessment and Remediation, University of South Australia, Mawson Lakes, South Australia 5095, Australia (E.L., W.H.W.); and National Risk Management Research Laboratory, United States Environmental Protection Agency, Cincinnati, Ohio 45224 (K.G.S.)

ORCID IDs: 0000-0002-6492-1939 (F.P.C.B.); 0000-0003-0409-9012 (D.J.P.).

Plant species differ in response to high available manganese (Mn), but the mechanisms of sensitivity and tolerance are poorly understood. In solution culture, greater than or equal to 30 μM Mn decreased the growth of soybean (*Glycine max*), but white lupin (*Lupinus albus*), narrow-leafed lupin (*Lupin angustifolius*), and sunflower (*Helianthus annuus*) grew well at 100 μM Mn. Differences in species' tolerance to high Mn could not be explained simply by differences in root, stem, or leaf Mn status, being 8.6, 17.1, 6.8, and 9.5 mmol kg^{-1} leaf fresh mass at 100 μM Mn. Furthermore, x-ray absorption near edge structure analyses identified the predominance of Mn(II), bound mostly to malate or citrate, in roots and stems of all four species. Rather, differences in tolerance were due to variations in Mn distribution and speciation within leaves. In Mn-sensitive soybean, in situ analysis of fresh leaves using x-ray fluorescence microscopy combined with x-ray absorption near edge structure showed high Mn in the veins, and manganite [Mn(III)] accumulated in necrotic lesions apparently through low Mn sequestration in vacuoles or other vesicles. In the two lupin species, most Mn accumulated in vacuoles as either soluble Mn(II) malate or citrate. In sunflower, Mn was sequestered as manganite at the base of nonglandular trichomes. Hence, tolerance to high Mn was ascribed to effective sinks for Mn in leaves, as Mn(II) within vacuoles or through oxidation of Mn(II) to Mn(III) in trichomes. These two mechanisms prevented Mn accumulation in the cytoplasm and apoplast, thereby ensuring tolerance to high Mn in the root environment.

Manganese (Mn) is an essential element for plant growth, but its availability differs greatly in space and time, depending largely on the nature and amount of Mn minerals present and on the soil's pH and redox potential. With an elaborate chemistry, Mn forms complexes with many organic and inorganic ligands. In soils, Mn has three common oxidation states, Mn(II), Mn(III), and Mn(IV), which form hydrated oxides of mixed valency; Mn is present also as numerous carbonates, silicates, sulfates, and phosphates (Lindsay, 1979). Cationic Mn^{2+} is the most common form readily absorbed by plant roots (Clarkson, 1988). The toxicity of Mn occurs in acid or waterlogged soils high in Mn minerals.

Many plants have mechanisms to accommodate the large differences in Mn^{2+} in soils. At low available Mn, uptake is increased in some Poaceae by excretion of phytosiderophores of the mugineic acid family (Takahashi et al., 2003), with root phytase exudation also potentially important for acquisition of Mn when Mn availability is limited (George et al., 2014). Mechanisms in other plants include the ability of roots to decrease rhizosphere pH or excrete organic ligands (Neumann and Romheld, 2012; Lambers et al., 2015). However, the

[1] This work was supported by the Australian Research Council (Future Fellowship nos. FT100100337 to E.L. and FT120100277 to P.M.K. and Linkage Project no. LP100100800 to C.T.) and The University of Queensland (postdoctoral fellowship to M.C.H.-S.). Parts of this research were conducted at the XFM beamline at the Australian Synchrotron, Victoria, Australia (Project AS153/XFM/8467). MRCAT operations are supported by the U.S. Department of Energy (DOE) and the MRCAT member institutions. This research used resources of the Advanced Photon Source, a U.S. DOE Office of Science User Facility operated for the DOE Office of Science by Argonne National Laboratory under Contract no. DE–AC02–06CH11357.

* Address correspondence to p.kopittke@uq.edu.au.

The author responsible for distribution of materials integral to the findings presented in this article in accordance with the policy described in the Instructions for Authors (www.plantphysiol.org) is: Peter M. Kopittke (p.kopittke@uq.edu.au).

F.P.C.B. and P.M.K. conceived the research plans; F.P.C.B. and M.C. conducted the plant-growth experiments; F.P.C.B., M.C.H.-S., M.C., C.T., D.J.P., and P.M.K. conducted the analyses at the Australian Synchrotron; E.L., K.G.S., and P.M.K. conducted the analyses at the Advanced Photon Source; W.H.W. and E.L. developed the procedure with LC-MS; F.P.C.B. and P.M.K. wrote the article with contributions from all other authors.

[OPEN] Articles can be viewed without a subscription.

www.plantphysiol.org/cgi/doi/10.1104/pp.15.00726

relative importance of the many complexes on Mn uptake remains unclear. Toxicity results from high Mn in leaf cell walls (Wissemeier et al., 1992; Wissemeier and Horst, 1992) and through adverse effects on symplastic proteins (Führs et al., 2008). Many plants have mechanisms that limit the adverse effects of high Mn^{2+} in soils, with numerous ligands involved in its translocation and that of other essential cations (Haydon and Cobbett, 2007). Edwards and Asher (1982) classified a range of crop and pasture species based on their ability to deal with high Mn as those that (1) limit Mn from entering the roots, (2) retain Mn in the roots, or (3) tolerate high Mn in the shoots. At the extreme are plants that hyperaccumulate more than 10,000 mg Mn kg^{-1} on a dry mass (DM) basis in foliar tissues without metabolic damage (Fernando et al., 2013; van der Ent et al., 2013). Based on 15% DM of leaves, this equates to 12.1 mmol kg^{-1} on a fresh mass (FM) basis. *Celosia argentia*, a species adapted to growth on Mn-contaminated mine tailings, accumulated more than 20,000 mg kg^{-1} Mn in leaves (Liu et al., 2014). Tolerance of high Mn in shoots of some Mn hyperaccumulators has been found to occur through binding to ligands (such as malate or citrate) or sequestration in the vacuole (Fernando et al., 2010).

Characteristic symptoms of Mn toxicity include chlorotic and distorted leaves with small necrotic lesions. These lesions have been shown in cowpea (*Vigna unguiculata*) to contain oxidized Mn and callose (Wissemeier et al., 1992), which forms as a reaction to high intracellular Ca (Kartusch, 2003). The necrotic lesions result mainly from oxidized phenolics (Wissemeier and Horst, 1992) and increased peroxidase activity in the apoplast (Horst et al., 1999). With a critical solution concentration for toxicity (10% growth reduction) of no more than 9 μM Mn, Edwards and Asher (1982) found that cotton (*Gossypium hirsutum*), bean (*Phaseolus vulgaris*), cowpea, and soybean (*Glycine max*) were the most sensitive species of 13 crop and pasture plants grown for 18 to 31 d at constant Mn in solution culture. By contrast, the critical concentration for sunflower (*Helianthus annuus*) was 7 times higher at 65 μM Mn. Sunflower was the first species found to tolerate high Mn through its sequestration in the trichomes on stems, petioles, and leaves (Blamey et al., 1986). The suspected accumulation of Mn was confirmed using wavelength dispersive x-ray spectroscopy with darkening inferred as due to insoluble higher oxides of Mn. Similarly, high Mn results in darkened trichomes of cucumber (*Cucumis sativus*) leaves due to oxidized Mn, as shown by the colorimetric benzidine test (Horiguchi, 1987). Watermelon (*Citrullus lanatus*; Elamin and Wilcox, 1986b), but not muskmelon (*Citrullus melo*; Elamin and Wilcox, 1986a), grown at high Mn also develops small dark spots around the leaf trichomes. Other species that sequester Mn in the trichomes include common nettle (*Urtica dioica*; Hughes and Williams, 1988) and *Alyssum murale*, a Ni hyperaccumulator (Broadhurst et al., 2009; McNear and Küpper, 2014). Thus, some plants in four families, Asteraceae, Cucurbitaceae, Urticaceae, and Brassicaceae, tolerate high Mn in shoots through Mn sequestration in or around the trichomes. The mechanisms may differ, however, because the high Mn present during development of common nettle stinging hairs decreases as plants mature (Hughes and Williams, 1988).

Recently developed techniques, including those based on synchrotron radiation, allow investigations of the distribution and speciation of Mn in planta, with most research to date focused on Mn hyperaccumulators (Fernando et al., 2013). For example, Fernando et al. (2010) used x-ray absorption near-edge spectroscopy (XANES) to confirm the widely accepted view that Mn(II) predominates in seven Mn hyperaccumulators. Synchrotron-based x-ray fluorescence microspectroscopy (μ-XRF) was used by McNear and Küpper (2014) to show that the basal region of trichomes of *A. murale* plants grown at no more than 10 μM Mn contained Mn(II) complexed with phosphate. At 50 μM Mn in solution, however, the increased amount of Mn that had accumulated around the trichomes was present as Mn(III). Few studies, however, have used synchrotron-based techniques to investigate the mechanisms of Mn toxicity and tolerance in agronomic species despite their importance for food production in regions where soils are acidic or intermittently waterlogged. One study on cowpea, with a critical toxicity concentration of only 2 μM Mn (Edwards and Asher, 1982), has shown an accumulation of Mn-citrate in the root cap and associated mucigel within 5 min of exposure to 150 μM Mn (Kopittke et al., 2013).

This study aimed to determine the distribution and speciation of Mn in fresh roots, stems, and leaves of four crop species, soybean, white lupin (*Lupinus albus*), narrow-leafed lupin (*Lupinus angustifolius*), and sunflower, which differ in tolerance to high Mn. It was hypothesized that Mn distribution and speciation would differ between Mn-sensitive soybean and the three other species. Furthermore, we considered it likely that the Mn tolerance mechanism of sunflower would differ from those of the two lupin species, which do not have darkened trichomes when grown at high Mn.

RESULTS

Plant Growth and Mn Status

Of the four plant species, only soybean was adversely affected when grown at high Mn, with small necrotic lesions forming after 3 d (Supplemental Fig. S1). Soybean DM decreased from 2.65 g $plant^{-1}$ at 0.5 μM Mn to 2.06 and 1.58 g $plant^{-1}$ at 30 and 100 μM Mn, respectively (Supplemental Table S1). By contrast, the white lupin, narrow-leafed lupin, and sunflower plants grew well at the three Mn levels (Supplemental Table S1), and there were no symptoms of Mn toxicity. There was a profusion of linear glandular trichomes and larger nonglandular trichomes (NGTs) on sunflower stems, petioles, and leaf blades (Supplemental Fig. S2, A and B; Aschenbrenner et al., 2013). Darkened NGTs were visible on petioles and leaves of sunflower plants 8 d after

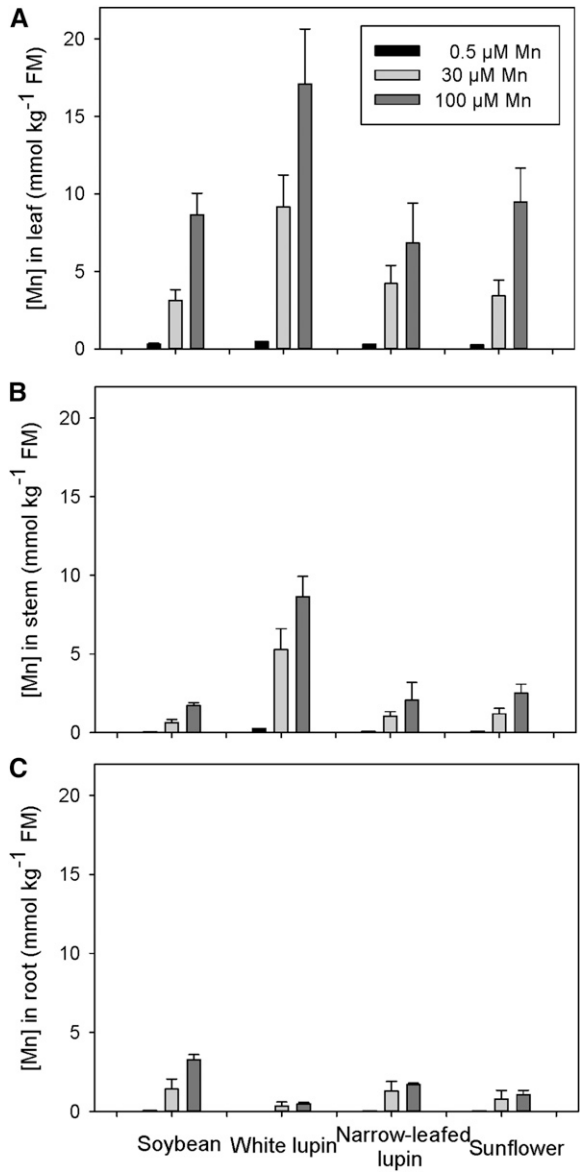

Figure 1. Concentration of Mn on a FM basis in leaf (A), stem (B), and root tissues (C) of soybean, white lupin, narrow-leafed lupin, and sunflower grown for 16 d in solutions containing 0.5, 30, or 100 μM Mn. Values are means ± SE (n = 2).

imposing the 100 μM Mn treatment (Supplemental Fig. S2C) and 3 d later at 30 μM Mn; no darkening of NGTs was evident at 0.5 μM Mn.

An increase in Mn in solution increased the concentration of Mn in tissues of all species, especially in leaves and shoots (Fig. 1). At 100 μM Mn, the highest Mn concentration of 17.1 mmol kg^{-1} FM was in leaf tissue of white lupin plants; the other species had approximately 50% of this, being 8.6, 6.8, and 9.5 mmol kg^{-1} FM in leaves of soybean, narrow-leafed lupin, and sunflower, respectively (Fig. 1A). The Mn concentration in white lupin equates to 14,100 mg kg^{-1} DM, exceeding the 10,000 mg kg^{-1} DM limit set by van der Ent et al. (2013) for leaves of plants that hyperaccumulate Mn. All species had a lower Mn concentration in the roots than in the tops at all Mn levels (Fig. 1C), with soybean containing 40% of total plant Mn content in the roots, while white lupin had 5% of total plant Mn in the roots. Thus, the severe effects of Mn toxicity in soybean (Supplemental Fig. S1, D–F) could not be ascribed simply to higher Mn in roots, stems, or leaves.

Plant Ca status in response to high Mn was investigated given its role in callose formation (Kartusch, 2003), which Wissemeier et al. (1992) found in Mn-toxic lesions of cowpea leaves. The Ca concentration in white lupin leaves and stems was significantly lower than in those of the other species, with high Mn decreasing the Ca concentration in stems of the two lupin species (Supplemental Fig. S3, A and B). On average, 100 μM Mn in solution decreased the Ca concentration in roots by 30% (Supplemental Fig. S3C). There were no consistent effects of elevated Mn in solution on the concentrations of Mg, K, P, S, Fe, Cu, or Zn in leaves, stems, or roots (data not shown).

Mapping Elemental Distribution

Despite the low Mn concentration in leaves of plants grown at 0.5 μM Mn, μ-XRF analysis of these control plants indicated Mn accumulated in small, localized areas throughout the leaf blade in soybean and near the leaf margins in white lupin and narrow-leafed lupin (Supplemental Fig. S4, A and B). The Mn was generally below the detection limit in sunflower (for more information, see Supplemental Results S1).

At 100 μM Mn, μ-XRF analyses indicated markedly different patterns of Mn accumulation in the leaves of the four plant species. In soybean, Mn accumulated near the veins and in localized areas of the leaf blade that were necrotic (Fig. 2A; Supplemental Fig. S5, A and B). There was marked variation in the relative Mn concentration across the leaf (Fig. 2B), with high Mn in the necrotic lesions and in or near the veins. These findings were confirmed at higher magnification (Fig. 2C and D; Supplemental Fig. S5C), with clear evidence of high Mn in or near the veins and especially in the necrotic lesions. The Mn concentration in the necrotic lesions was often 100- to 1,000-fold higher than in the surrounding tissue (Fig. 2D), with many regions below the detection limit in the undamaged areas of the leaf blade. Rather than this simple contrast between regions of high and low Mn, further analysis of the μ-XRF Ca and Mn data revealed a complex subcellular distribution of Mn (Fig. 3A). The necrotic lesions had a high Ca concentration, again in marked contrast to that in undamaged areas of the leaf blade (Supplemental Fig. S6A). High Ca was evident also as small spots (typically 5–10 μm) in the undamaged leaf blade (Supplemental Fig. S6B), the spots being interpreted as vacuoles where high Ca accumulates. It is possible to use Ca concentration as an indicator of subcellular distribution given

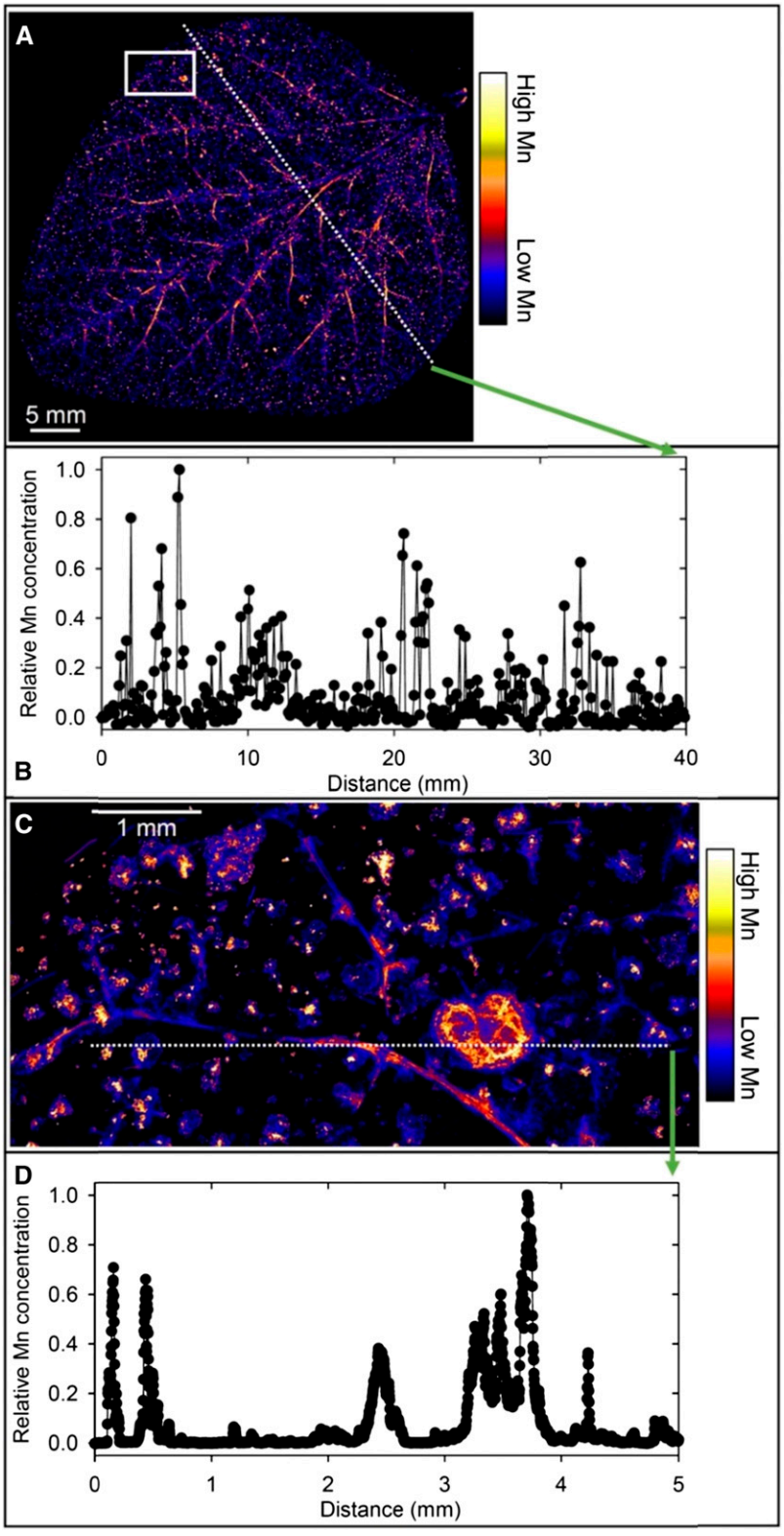

Figure 2. Compton-corrected μ-XRF images of Mn in a leaf of a soybean plant grown for 16 d at 100 μM Mn. A, Overview of a whole leaf illustrating Mn distribution along major veins and in localized areas. B, Relative Mn concentration along the transect identified in A. C, Detailed Mn distribution in a leaf section identified by the white box in A. D, Relative Mn concentration along the transect identified in C illustrating Mn accumulation in localized necrotic areas and in or near the veins.

that Ca in the vacuole (1–80 mM) is often 10,000-fold higher than in the cytoplasm (100 nM; Stael et al., 2012). There was a clear difference between Ca and Mn distribution in this region, with no vacuolar Mn evident (Supplemental Fig. S6, B and C).

In white lupin, there was a high accumulation of Mn toward the edge of the leaf blade from a plant grown at 100 μM Mn (Fig. 4A), there being a consistent increase in Mn of greater than 3-fold from near the midrib to the outer edges of the leaf (Fig. 4B). Page et al. (2006) reported

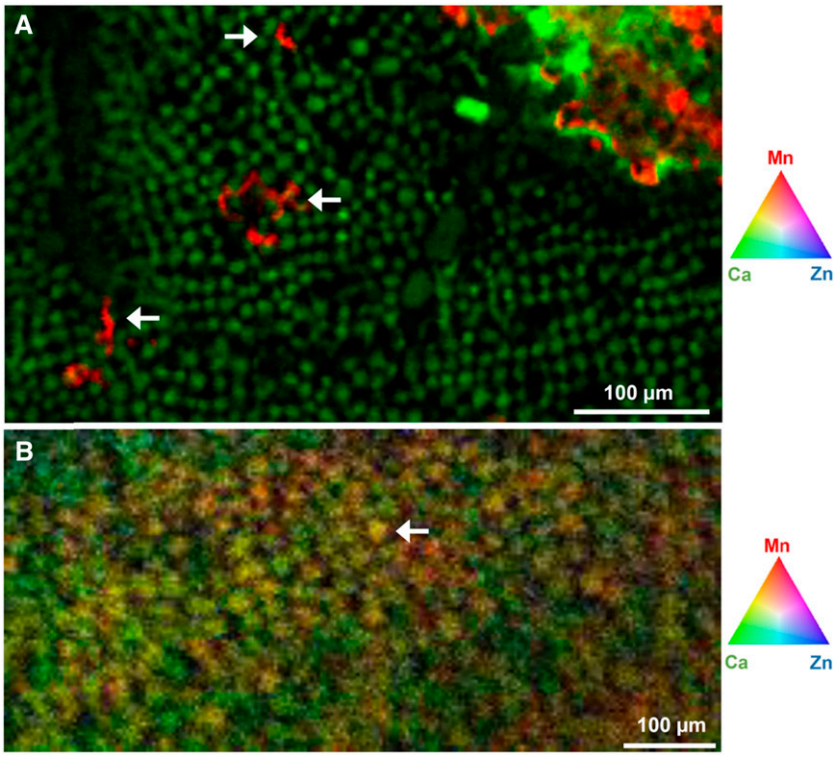

Figure 3. Distribution of Ca and Mn in parts of soybean and narrow-leafed lupin leaves. A, In soybean, Ca is located in vacuoles of cells in undamaged areas of the leaf with Mn visible in a lesion (top right) and in incipient necrotic lesions identified by the three white arrows in A. B, In narrow-leafed lupin, Ca and Mn are colocated in vacuoles as illustrated by the white arrow in B. For more detail, see Supplemental Figures S6 and S7.

a similar finding in white lupin using ^{54}Mn. At higher magnification, it was evident that Mn varied near the leaf edge by approximately 5-fold, being higher and rather evenly distributed in the interveinal areas (Fig. 4, C and D). It is noteworthy that Mn did not decrease to a level below the detection limit (Fig. 4, B and D), as occurred in soybean (Fig. 2, B and D). Overall, therefore, there was higher Mn toward the leaf edge in white lupin leaves but little accumulation in or near the veins.

In some respects, specifically regarding Mn accumulation near the leaf edge, Mn accumulation in narrow-leafed lupin at 100 μM Mn (Fig. 5A) was similar to that in white lupin. However, high Mn near the leaf edge occurred in patches, and there was even higher Mn near the leaf tip. As with white lupin, Mn was 3- to 5-fold higher near the leaf edge than near the midrib (Fig. 5B). Higher magnification of a selected area near the edge of the leaf (Fig. 5C) illustrated only an approximately 2-fold change in Mn within an area of high Mn (Fig. 5D). The Mn concentration at the leaf tip, however, was up to 50 times that in the Mn patches further away from the tip (data not shown), as might be expected with Mn(II) carried in the transpiration stream (Page et al., 2006) in a leaf with a prominent midrib but sparse and filamentous lower order veins. Further analysis of μ-XRF Ca and Mn data revealed a more complex pattern than first surmised. As with soybean, high Ca was located in small spots (typically 15–20 μm), interpreted as vacuoles (Supplemental Fig. S7, A and B). Unlike soybean, Mn was distributed in these same spots (Supplemental Fig. S7C), indicating sequestration of both Ca and Mn in narrow-leafed lupin vacuoles (Fig. 3B; Supplemental Fig. S7D) possibly via the same transporter (Millaleo et al., 2010).

The pattern of Mn distribution in a leaf of sunflower grown at 100 μM Mn (Fig. 6A) differed greatly from those of the other three species, with high Mn associated with the NGTs across the leaf blade and at its edge but not in the leaf blade itself. As with soybean (Fig. 2, B and D), Mn in the leaf blade was largely below the detection limit, the associated variability ranging over many orders of magnitude (Fig. 6B). The high Mn associated with the NGTs was more clearly illustrated at higher magnification of a selected area close to the leaf edge (Fig. 6C). In this instance, marked changes in relative Mn concentration occurred over distances of less than 0.1 mm, with the Mn concentration in the trichomes greater than 1,000-fold higher than that in the leaf blade (Fig. 6D). Furthermore, Mn was many times higher at the base than further along the NGT, as illustrated by a traverse along the middle of a trichome (Supplemental Fig. S8).

Further attention was given to Ca distribution in leaf tissue in view of the effects of elevated Mn in solution on plant Ca status (Supplemental Fig. S3). There was high Ca and Mn in necrotic lesions due to Mn toxicity in soybean at 100 μM Mn (Supplemental Fig. S9, A and B). Interestingly, however, Mn accumulated in or near the veins, where Ca was below the detection limit. Furthermore, high Mn but not high Ca was present in the

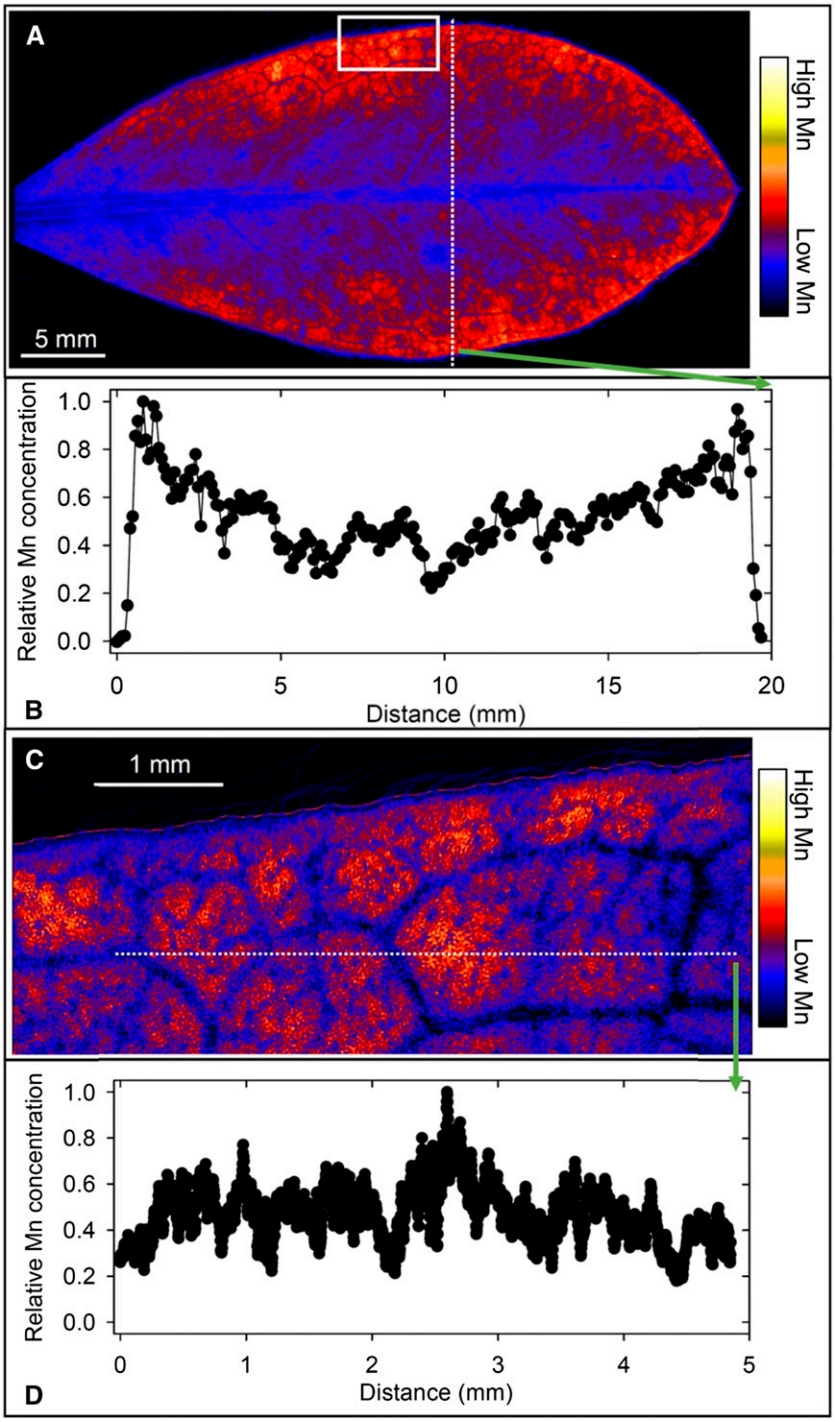

Figure 4. Compton-corrected μ-XRF images of Mn in a leaf of a white lupin plant grown for 16 d at 100 μM Mn. A, Overview of a whole leaf illustrating higher Mn toward the leaf edge. B, Relative Mn concentration along the transect identified in A illustrating the increase from the midvein to the leaf edge. C, Detailed Mn distribution in a leaf section identified by the white box in A, with low Mn near the veins and high Mn in the interveinal areas. D, Relative Mn concentration along the transect identified in C illustrating the variation near the leaf edge.

incipient necrotic lesions within the undamaged leaf blade (Fig. 3; Supplemental Fig. S6D). At the resolution of Supplemental Figure S9, there was no close association between Mn and Ca in the two lupin species. In white lupin, Mn was spread throughout the leaf blade, notably toward the leaf edge but not in or near the veins, while high Ca was located primarily in the trichomes at the leaf edge (Supplemental Fig. S9, C and D). In narrow-leafed lupin, there was lower Ca in the region of highest Mn accumulation near the edge of the leaf (Supplemental Fig. S9, E and F). In contrast to these three species, both Mn and Ca were highest in sunflower NGTs (Supplemental Fig. S9, G and H). Closer examination revealed that most Mn was towards the base of the trichome (Supplemental Fig. S9G), as might be interpreted from the darkened NGTs (Supplemental Fig. S2C), while high Ca was nearer the tip of the trichome in many instances (Supplemental Fig. S9H).

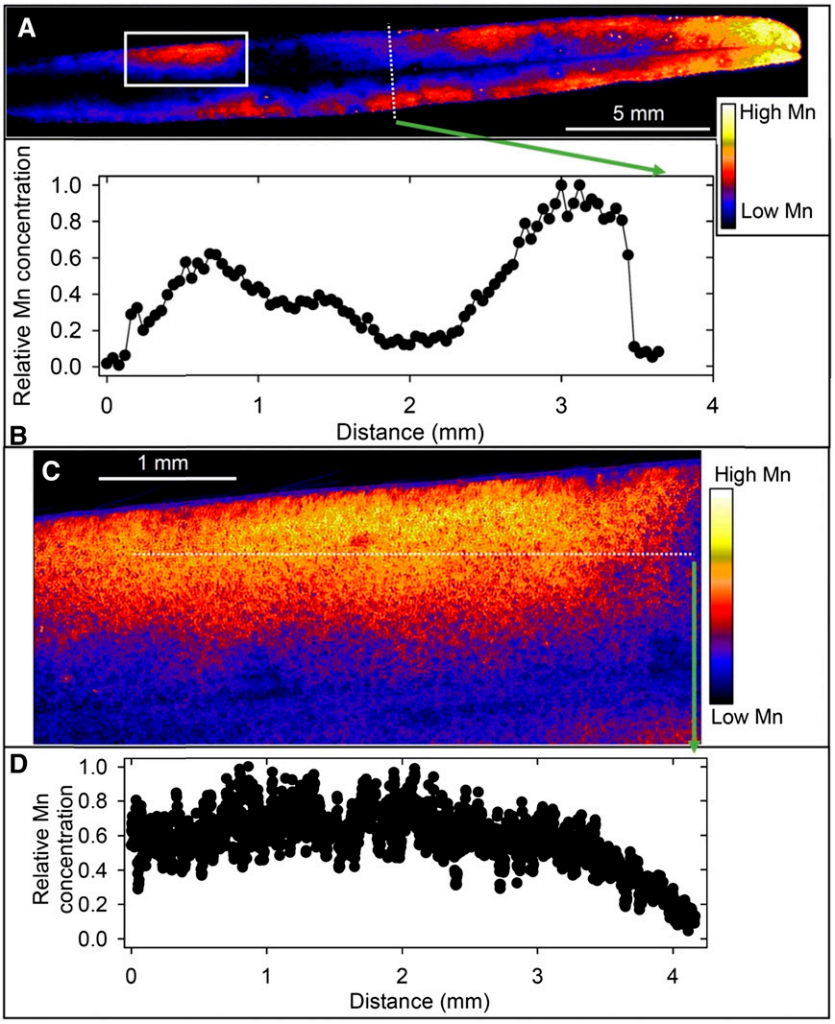

Figure 5. Compton-corrected μ-XRF images of Mn in a leaf of a narrow-leafed lupin plant grown for 16 d at 100 μM Mn. A, Overview of a whole leaf illustrating high Mn in patches near the leaf edge and especially toward the tip. B, Relative Mn concentration along the transect identified in A illustrating the increase from the midvein to the leaf edge. C, Detailed Mn distribution in a leaf section identified by the white box in A. D, Relative Mn concentration along the transect identified in C illustrating the variation in Mn accumulation near the leaf edge.

Although μ-XRF analyses in this study focused on leaves where high Mn exerts its toxic effects (Wissemeier and Horst, 1992), the distribution of Mn was determined also in the roots of the four plant species grown at 100 μM Mn. Overall, Mn was highest in narrow-leafed lupin roots (Supplemental Fig. S10), as found in the analysis of bulk roots (Fig. 1C). In particular, there was high Mn at the root apex and in the older root tissues, with lower Mn in the tissues immediately behind the apex. Quantitative analysis determined that Mn was located preferentially in the rhizodermis of the four species, with at least 10 times more Mn in the rhizodermis of narrow-leafed lupin than in that of the other species (Supplemental Fig. S11).

As hypothesized, Mn in a sunflower leaf increased substantially 1 d after plant transfer from 0.5 to 100 μM Mn (Supplemental Fig. S12). An overview scan of a leaf grown continuously at 0.5 μM Mn indicated that Mn was associated with NGTs (Supplemental Fig. S12, A and D). Even at this 0.5 μM Mn in solution, Mn accumulated at the trichome base (Supplemental Fig. S12, B and E) and increased substantially after only 1 d at 100 μM Mn (Supplemental Fig. S12, C and F). Accumulation of Mn was evident at the base of the trichomes, while Ca dominated toward their tips.

Manganese Speciation in Plant Tissues

The oxidation state of Mn was a major discriminant in the XANES spectra of the standard compounds (Supplemental Fig. S13), with the white-line peak being approximately 6,552 eV for Mn(II) compounds and approximately 6,560 eV for Mn(III) and Mn(IV). While these changes in oxidation states were easily distinguished due to shifts in the white-line peak, there were only minor differences in the spectra for the Mn(II) compounds (aqueous Mn, Mn citrate, Mn malate, and Mn oxalate). For aqueous Mn and Mn oxalate, although the differences were small, they were sufficient to allow discrimination (Supplemental Fig. S14). However, given the close similarity of the spectra for Mn citrate and Mn malate (Supplemental Fig. S14), we did not distinguish between these two compounds when later doing linear combination

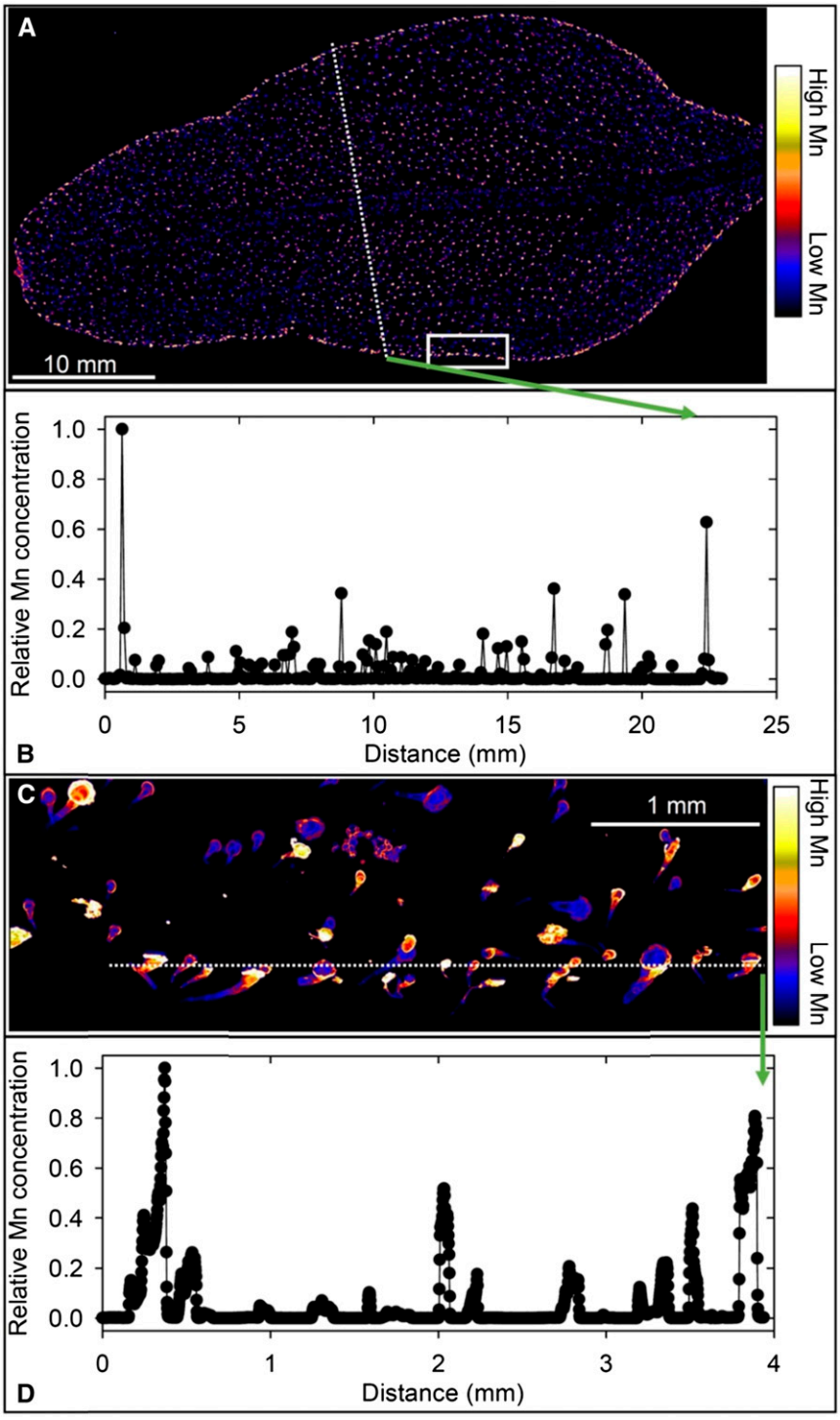

Figure 6. Compton-corrected μ-XRF images of Mn in a leaf of a sunflower plant grown for 16 d at 100 μM Mn. A, Overview of a whole leaf illustrating Mn accumulation associated with NGTs. B, Relative Mn concentration along the transect identified in A illustrating the variation in Mn accumulation. C, Detailed Mn distribution in a leaf section identified by the white box in A. D, Relative Mn concentration along the transect identified in C illustrating high Mn accumulation in NGTs.

fitting (LCF). Results of liquid chromatography (LC)-mass spectrometry (MS) analysis showed that concentrations of citrate and malate exceeded that of oxalate in tissues of the four species (Supplemental Table S2), which was below the detection limit. Citrate was higher than that of malate in roots, especially in the lupin species. Except for soybean, malate was higher in the stems and leaves, especially in white lupin. Sunflower had low concentrations of both organic ligands in all tissues.

We examined the speciation of Mn in plant tissues using two approaches. First, laterally resolved data on the speciation of Mn within plant tissues was obtained using the Maia detector system at the Australian Synchrotron. With fluorescence-XANES imaging, speciation data (i.e., XANES spectra) were collected for every

pixel in the map as explained by Kopittke et al. (2014). This procedure differs from the typical approach of obtaining micro-XANES spectra at specific individual locations. However, fluorescence-XANES imaging has lower sensitivity than bulk x-ray absorption spectroscopy (XAS), which was was used in our second approach at the Advanced Photon Source.

We used florescence-XANES imaging to examine Mn in the undamaged areas and in adjacent necrotic lesions in leaves of soybean grown at 100 μM Mn. The Mn in the background leaf tissue was below the detection limit, precluding speciation analysis. Furthermore, all Mn within the necrotic lesions in soybean leaves appeared to be of a single form, as did Mn in leaves of the two lupin species (data not shown). This indicates that better data would be obtained using XAS given its higher sensitivity.

Fluorescence-XANES imaging was used to examine the trichomes of sunflower grown at 100 μM Mn. Pixel populations were identified as differing in Mn speciation in a single trichome (Fig. 7; Supplemental Fig. S15A) using the energy association module in GeoPIXE (Kopittke et al., 2014). Three Mn populations (other than the background pixels) were identified in which Mn concentration changed from the base to the tip (Fig. 7; Supplemental Fig. S15). The XANES spectra extracted from the population of pixels at the base of the trichome (Supplemental Fig. S15, A and D, Population 1) had a white-line peak at approximately 6,560 eV, which corresponds to oxidized forms of Mn, with a shoulder at approximately 6,552 eV corresponding to Mn(II; Fig. 7C). Using LCF, it was predicted that 66% of the Mn at the base of the trichome was present as manganite, with the remaining Mn present as aqueous Mn(II). The similarity of the Mn(II) spectra (Supplemental Fig. S13) and the comparatively low sensitivity of the XANES imaging technique prevented the determination as to whether the remaining Mn(II) was aqueous Mn^{2+} or complexed by simple organic ligands. In pixel populations further along the trichome (Supplemental Fig. S15A), there was a decrease in the peak at 6,560 eV, indicating a decreased proportion of manganite with distance from the base of the trichome (Fig. 7C). This was coupled with an increase of Mn(II) compounds at 6,552 eV. It was estimated from LCF analysis that manganite decreased from 66% in Population 1 to 10% and 5% in Populations 2 and 3 (Fig. 7B). With this decrease in manganite in Populations 2 and 3, there was a concomitant increase in soluble Mn(II) to approximately 90% of the Mn present.

Using bulk XAS, the Mn spectra for the roots showed that Mn speciation was similar in all four species, with the white-line peak at 6,552 eV indicating soluble Mn(II) forms (i.e. aqueous Mn, Mn citrate, Mn malate, or Mn oxalate; Fig. 8). This was confirmed using LCF analysis, which indicated Mn(II) malate or citrate to be the dominant form in all four species: 87% in soybean and narrow-leafed lupin, 90% in white lupin, and 91% in sunflower (Supplemental Table S3). The form of the remaining 9% to 13% of the Mn was unclear, with only

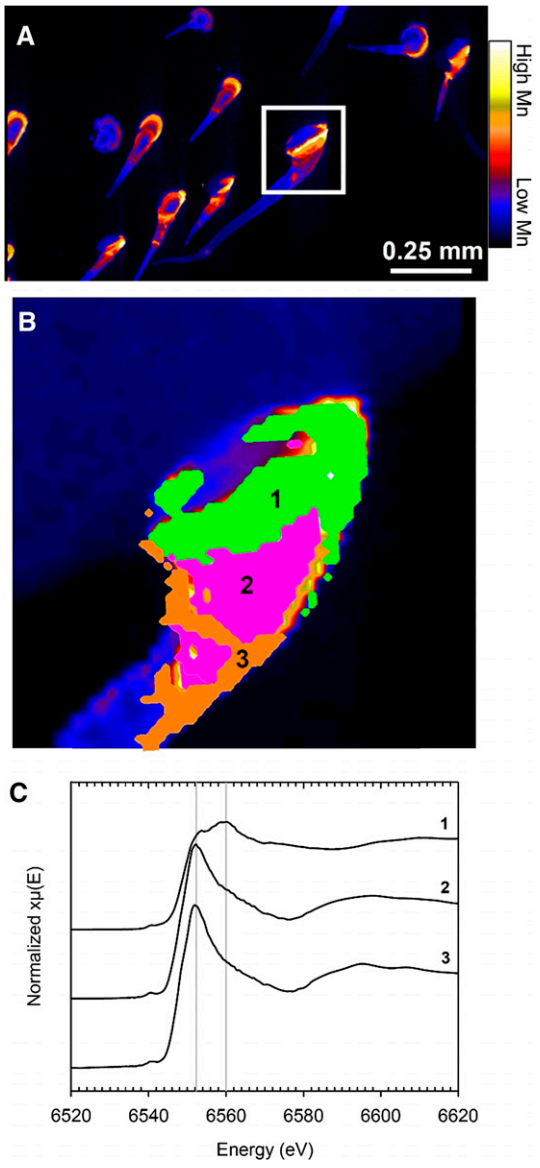

Figure 7. Distribution of Mn in part of a leaf blade and in NGTs of a sunflower leaf grown for 16 d at 100 μM Mn. A, High Mn is present mostly at bases of NGTs. B, Close-up of the base of a trichome identified by the white box in A that was examined using XANES imaging overlaid with the three pixel populations identified using the energy association module in GeoPIXE as shown in Supplemental Figure S15. C, Average XANES spectra extracted from the three pixel populations identified in B.

small variations in the R-factor when the remaining ligand was varied widely (data not shown). For example, in narrow-leafed lupin, the R-factor changed from 0.00864 to 0.00879 when the ligand was Mn_2O_3 instead of manganite. The speciation of Mn in stems was similar to that in the roots of all species, with Mn(II) malate or citrate accounting for 74% to 86% of the Mn (Fig. 8; Supplemental Table S3). Again, speciation of the remaining Mn (14%–26%) was unclear.

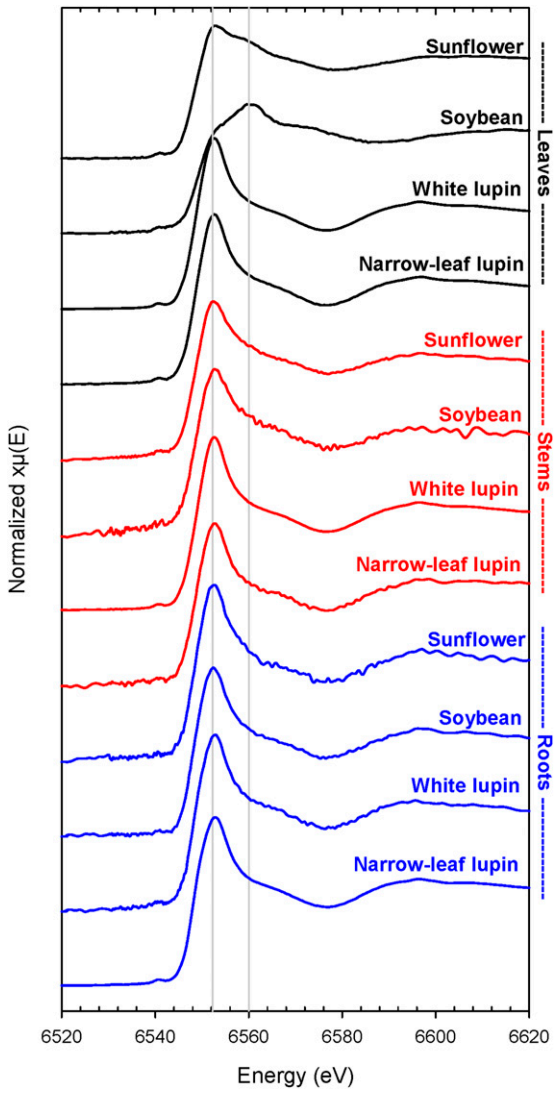

Figure 8. Normalized K-edge XANES spectra for freeze-dried leaves, stems, and roots of soybean, white lupin, narrow-leafed lupin, and sunflower grown for 16 d at 100 μM Mn. To allow comparison, the vertical lines correspond approximately to the white-line peaks of Mn (II; 6,552 eV) and Mn(III) and Mn(IV; 6,560 eV).

In contrast to the roots and stems, XAS analyses of bulk leaf tissues identified marked differences in Mn speciation among the four plant species exposed to 100 μM Mn (Fig. 8; Supplemental Table S3). In soybean, the white-line peak corresponded to approximately 6,560 eV (i.e., oxidized Mn), with a shoulder at 6,552 eV, indicating soluble Mn(II). In the two lupin species, the position of the white-line peak corresponded to Mn(II), indicative of aqueous Mn, Mn citrate, Mn malate, or Mn oxalate. In sunflower, the white-line peak was at 6,552 eV [i.e., Mn(II)], but there was a shoulder at 6,558 to 6,560 eV for oxidized Mn.

In all species, therefore, it appears that Mn malate or citrate was present in and translocated through roots and stems. LCF analysis showed that Mn malate or citrate was the dominant form in leaves of the two lupin species, being 84% of the Mn in white lupin and 85% in narrow-leafed lupin (Supplemental Table S3). In both soybean and sunflower, however, it was concluded that Mn(II) in roots and stems was oxidized to Mn(III) to varying extents in the leaves. Using LCF analysis, manganite was predicted to account for 66% of the total Mn in soybean leaves, with the form of the remaining Mn unclear. In sunflower, 43% of the Mn was attributed to manganite, with the remainder as Mn(II), either as aqueous Mn or bound to simple organic ligands.

DISCUSSION

This study with four crop species used synchrotron-based techniques in combination with plant growth response, visible symptoms, and measured Mn status to investigate the mechanisms of sensitivity and tolerance to high Mn in the root environment.

XAS analyses determined that Mn(II) dominated in roots of all species grown at 100 μM Mn (Fig. 8), despite their differences in tolerance to high Mn. Soybean had the highest quantity of Mn in roots of the four species when grown at high Mn, retaining 40% of total plant Mn in roots as found by Edwards and Asher (1982). Of the species tolerant to high Mn, narrow-leafed lupin also retained high Mn (35%) in the roots, but white lupin and sunflower retained only 5% and 15%. The Mn in roots of the four species was mostly Mn(II) complexed by malate or citrate. This finding and that of LC-MS analysis is in keeping with that of Fernando et al. (2010), who concluded that malate or citrate is the most likely carboxylate to complex Mn in hyperaccumulators. Dou et al. (2009), however, determined oxalate to be important, a finding not supported by data for the species examined in this study. The concentration of Mn was considerably higher in the stems than in the roots and differed markedly among the four species. At 8.6 mmol kg^{-1} FM, white lupin grown at 100 μM Mn had the highest Mn concentration in stems, greater than 3-fold higher than that of the other three species (Fig. 1B). Analysis using XAS identified most Mn in shoots as Mn(II) complexed with malate or citrate, indicating Mn(II) to be the major form translocated via the xylem. This is consistent with the rapid uptake of Mn by cowpea (Kopittke et al., 2013) and the transport of ^{54}Mn via the transpiration stream in white lupin (Page et al., 2006). In this study, therefore, responses of species to high Mn were not related to Mn concentration or speciation in roots and stems. This, in turn, directed our focus to the leaves, where high Mn exerts its toxic effects in cowpea (Wissemeier and Horst, 1992; Führs et al., 2008).

The first question that arises is why does the effect of high Mn in soybean leaves differ from that in the other three species that tolerate high Mn? Clearly, this is not due simply to a high Mn concentration in soybean leaves that is approximately one-half of that in white lupin and similar to that in narrow-leafed lupin and sunflower (Fig. 1A). It is more likely that the difference

between soybean and the other species lies in the cellular distribution and speciation of Mn (Figs. 2–6). In soybean leaves, there was a marked localization of high Mn in or near the veins and especially in the necrotic lesions that were high in Mn(III). This was in marked contrast to the low Mn in the undamaged areas (Fig. 2, C and D). μ-XRF analysis indicated that Ca was located mostly in the vacuoles (Supplemental Fig. S6B), which Stael et al. (2012) concluded contain approximately 80 mM Ca compared with only approximately 100 nM in the cytoplasm. The concentration of Mn must be maintained at less than 100 nM in the cytoplasm also (Hughes and Williams, 1988), but in contrast to Ca, there was low Mn in the vacuoles but high in some intervening spaces (Fig. 3A; Supplemental Fig. S6C). The same transporter is often involved in Ca and Mn accumulation in the vacuole (Millaleo et al., 2010), suggesting that elevated Mn in the apoplast exceeds the limited capacity of the transporters required to meet the low Mn requirements in the cytoplasm. Alternatively, high Mn may enter the cytoplasm only to be retransported to the apoplast via exocytosis, which is a conserved mechanism for heavy metal tolerance in plants (Peiter et al., 2007). Hughes and Williams (1988) concluded that the eukaryotic cell pumps Mn into almost any vesicular partition of the cell rather than leave it in the cytoplasm, where high levels are toxic (Führs et al., 2008). High Mn in the veins further suggests the absence of an effective Mn sink in soybean leaves, with excess Mn remaining in or moving to the walls of cells in the interveinal regions where necrosis occurs through oxidation of phenolics (Wissemeier et al., 1992) and high peroxidase activity in the apoplast (Horst et al., 1999). Oxidation of Mn(II) to Mn(III) would be a likely consequence, as would be callose formation through cellular injury. The mechanisms causing the difference in vacuolar Mn and Ca in soybean clearly require further research.

The second question that arises is why does high Mn in the leaves of lupin species not result in toxicity? Taking narrow-leafed lupin grown at 100 μM Mn as an example, high Mn accumulated in patches near the edge of the leaf (Fig. 5, A and B), with moderate variation in Mn concentration within these areas of high Mn (Fig. 5, C and D). Examination of Ca and Mn distribution (Supplemental Fig. S7, B and C) showed that these two elements were colocated in the vacuoles (Fig. 3B), thereby ensuring low cytoplasmic concentrations of Ca (Stael et al., 2012) and Mn (Hughes and Williams, 1988; Peiter et al., 2007). This suggests that narrow-leafed lupin is able to translocate Mn(II) from the apoplast for storage in the vacuole, possibly via a Ca transporter (Millaleo et al., 2010), limiting the accumulation of Mn in the cytoplasm and cell wall. A similar mechanism would occur in white lupin also (data not shown). Using XANES, Fernando et al. (2010) concluded that Mn(II) predominates in Mn hyperaccumulators, with Fernando et al. (2008) being the first to show that Mn is evenly distributed in leaf photosynthetic and nonphotosynthetic tissues. White lupin would be classified as a Mn accumulator (van der Ent et al., 2013) by growing well at 100 μM Mn, with leaves containing 17.1 and 25.0 mmol Mn kg^{-1} FM (14,100 and 20,700 mg Mn kg^{-1} DM; Fig. 1; Supplemental Fig. S16). This finding of vacuolar Mn accumulation differs from that suggested by Page et al. (2006), who attributed the high ^{54}Mn in leaves of white lupin to result from restricted loading of the phloem or accumulation of insoluble Mn.

The third question is why does manganite [Mn(III)] in sunflower NGTs limit the toxic effect of Mn? Many studies have identified trichomes as sites of metal accumulation, with Broadhurst et al. (2004), for example, reporting high levels of Ni, Mn, and Ca in trichomes of *A. murale*. Despite a marked difference in trichome morphology, sunflower NGTs accumulated Mn and Ca when grown at 100 μM Mn in solution (Figs. 6 and 7). With Mn present at a concentration below the detection limit in the leaf blade (Fig. 6C), we conclude that sunflower has a mechanism whereby Mn(II) is translocated via the apoplast to the NGT, where it is oxidized to insoluble manganite. Such a mechanism would limit Mn(II) accumulation in the cytoplasm and in the cell wall, where it is toxic (Hughes and Williams, 1988; Wissemeier and Horst, 1992; Führs et al., 2008). It is unclear, however, if this mechanism is the same as has been demonstrated in a number of plant species that accumulate high Mn in trichomes (Elamin and Wilcox, 1986b; Horiguchi, 1987; Hughes and Williams, 1988; Broadhurst et al., 2009; McNear and Küpper, 2014). For example, deposition of Mn by phosphate and conversion to Mn(III) have been implicated in tolerance to high Mn by *A. murale* (McNear and Küpper, 2014). Uncertainty remains also as to the subcellular location of manganite, other than its basal accumulation in sunflower NGTs (Fig. 7). Blamey et al. (1986) suggested an accumulation of Mn in and around the trichomes. However, manganite may be present in the vacuole, as found with Ni accumulation in trichomes of *Alyssum lesbiacum* (Küpper et al., 2001).

The fourth question is why is manganite associated with Mn toxicity in soybean but a sign of Mn tolerance in sunflower? We conclude that, in soybean, Mn accumulates in the apoplast through lack of a suitable Mn sink, resulting in oxidative damage and subsequent oxidation of Mn(II) to manganite. In sunflower, however, this study has indicated that a mechanism exists whereby oxidation to manganite at the base of NGTs limits Mn accumulation in the apoplast or cytoplasm, thereby preventing metabolic damage.

Finally, μ-XRF analysis demonstrated the efficiency of the Mn tolerance mechanism in sunflower, with Mn accumulation at the base of NGTs within 1 d of transfer to 100 μM Mn solution (Supplemental Fig. S12). This timeframe should be considered when further studying the mechanisms of high Mn effects.

CONCLUSION

Synchrotron-based techniques and others have provided detailed information relating to the mechanisms

whereby four crop species respond to high Mn in the root environment. Differences in response could not be ascribed simply to differences in Mn concentration in roots or stems, with XAS and LC-MS analyses indicating the predominance of Mn(II), mostly as Mn malate or Mn citrate, in all species grown at 100 μM Mn. Furthermore, differences in sensitivity or tolerance to high Mn could not be ascribed simply to differences in leaf Mn status.

The toxicity of Mn to soybean was first evident as visible necrotic symptoms followed by reduced growth. Necrotic lesions were shown by μ-XRF to be high in Mn and Ca, with high Mn in the veins also. This was in contrast to Mn below the detection limit in the undamaged interveinal areas. The presence of Ca but not Mn in the vacuoles indicated the lack of an efficient mechanism of Mn sequestration, in turn resulting in localized necroses and subsequent oxidation of Mn(II) to manganite in the walls of cells in the interveinal regions.

Mn(II) was distributed throughout the leaves of the two lupin species, with a moderate increase toward the leaf edges. Interestingly, Mn was low in or near the veins, even in regions of high Mn in white lupin; indistinct venation precluded an assessment in narrow-leafed lupin. High Ca and Mn in the vacuoles of narrow-leafed lupin leaves suggest that high Mn(II) is translocated from the apoplast into the vacuoles, where it is nontoxic. The presence of manganite at the base of NGTs in sunflower was considered a tolerance mechanism by preventing Mn(II) accumulation in the cytoplasm or apoplast of leaf blade cells.

Overall, therefore, the microscopic distribution and speciation of Mn has provided insights into the mechanisms whereby four crop species respond to high Mn. The toxicity of high Mn in soybean resulted from Mn accumulation in leaf cell walls through an inability to sequester Mn in vacuoles or other vesicles. Two mechanisms of tolerance to high Mn in leaves were identified: sequestration of Mn malate or Mn citrate in vacuoles by the two lupin species and oxidation of Mn(II) to manganite at the base of sunflower NGTs. The biochemistries of these two tolerance mechanisms remain to be determined.

MATERIALS AND METHODS

Plant Growth, Elemental Mapping, and Laterally Resolved Speciation

A solution culture experiment was conducted following two preliminary experiments to establish appropriate control and high-Mn conditions for soybean (*Glycine max*) 'Bunya,' white lupin (*Lupinus albus*) 'Kiev mutant,' narrow-leafed lupin (*Lupinus angustifolius*) 'Mandelup,' and sunflower (*Helianthus annuus*) 'Hyoleic 41.' Seeds were germinated in rolled paper towels held vertically in tap water and 3-d-old seedlings transplanted into 33 L of aerated solution containing nominal concentrations of (μM): 1,000 Ca, 120 NH_4^+-N, 95 Mg, 300 K, 10 Na, 6 Fe, 0.5 Mn, 0.5 Zn, 0.2 Cu, 1,250 Cl, 670 NO_3^--N, 340 SO_4^{2-}-S, 5 PO_4^--P, 1 B, and 0.01 Mo at pH 5.6. A 10-mL aliquot of 0.0033 M KH_2PO_4 was added daily to ensure adequate P in solution. Solutions were replaced weekly, and three treatments of 0.5 (control), 30, and 100 μM Mn imposed after 4 d, with plants of all species grown in each of the three containers. Concentrations of selected nutrients in solution were determined at the start and end of each week using inductively coupled plasma optical emission spectroscopy, resulting in mean values ($n = 18$) of (μM): 990 Ca, 78 Mg, 190 K, 20 Na, 22 P, 350 S, 5.5 Fe, 0.11 Cu, and 0.36 Zn. The mean concentration ($n = 6$) of Mn was 0.5, 26, and 92 μM in the nominal 0.5, 30, and 100 μM Mn treatment solutions.

The plants were grown at 25°C under fluorescent lights in a controlled environment room at the Centre for AgroBioscience (La Trobe University) and for the final 4 d at 22°C in a laboratory at the Australian Synchrotron under high-pressure sodium lights. This arrangement permitted sampling and mounting of fresh leaf and root tissues, with a delay of less than 5 min between excision and the start of μ-XRF analyses. At the end of the experimental period, plants were harvested and separated into root, stem plus petiole, and leaf. The FM and DM at 65°C of these plant parts were determined and then ground and digested in perchloric acid:nitric acid (1:5) to measure concentrations of Mn and of Ca, Mg, K, Na, Fe, Cu, Zn, P, and S in bulk tissues by inductively coupled plasma optical emission spectroscopy. (Nutrient concentrations are presented on an FM basis because μ-XRF analyses were carried out on fresh tissue but may be converted to a DM basis using data in Supplemental Table S4).

Details of the x-ray fluorescence microscopy (XFM) beamline at the Australian Synchrotron have been described by Paterson et al. (2011). Kopittke et al. (2011) have provided information on operating conditions for the study of fresh plant material. Briefly, x-rays were selected by a Si(111) monochromator and focused (approximately 2 μm × 2 μm) on the specimen by a pair of Kirkpatrick-Baez mirrors. The x-ray fluorescence emitted by the specimen was collected using the 384-element Maia detector system in a backscatter position at an excitation energy of 12,700 eV. Specimens consisted of whole or parts of leaf blades and the apical 30-mm sections of roots mounted between two 4-μm Ultralene films to provide support and limit dehydration. Elemental mapping of each specimen involved continuous on-the-fly analysis in the horizontal direction and discrete steps in the vertical direction. The step size and stage velocity varied as outlined below. The full x-ray fluorescence spectra were analyzed using the CSIRO Dynamic Analysis method in GeoPIXE (http://www.nmp.csiro.au/dynamic.html), which enables quantitative, true-elemental images (Ryan and Jamieson, 1993; Ryan, 2000). These scans provide two-dimensional representations (i.e., areal concentrations) of three-dimensional objects that vary in thickness. For the leaves, all μ-XRF images other than those in Supplemental Figure S4A have been normalized to the Compton scatter to correct for variation in leaf thickness and relative concentrations reported. μ-XRF images of roots were not corrected for variations in thickness across the root cylinder because projected volumetric concentrations were obtained by multiplying the areal concentration by the calculated relative thickness of the root at each selected point (Wang et al., 2013).

Three types of scans were carried out to examine the tissue samples. An initial survey scan was utilized to obtain an overview of the leaf and to identify an area of interest. These scans had a step size (i.e., pixel size) of 80 μm for the leaves and 6 μm for the roots. The horizontal stage velocity was 4.1 mm s^{-1} for both leaves and roots, resulting in a pixel transit time of approximately 20 ms. Depending upon the size of the scanned area, each survey scan typically took 20 to 60 min. Following the survey scan, a detailed scan was collected within a small area of interest with a step size of 2 μm for both leaves and roots. The horizontal stage velocity was 2.0 or 4.1 mm s^{-1}, resulting in a pixel transit time of approximately 0.5 or 1 ms. Each detailed scan typically took 30 to 60 min for these smaller areas of interest. For some tissues, a XANES imaging scan was used to provide laterally resolved data regarding the speciation of Mn. This XANES imaging scan consisted of 116 individual scans forming a stack of μ-XRF maps. These 116 scans were collected at decreasing incident energies from 6,690 to 6,510 eV across the Mn K-edge. To match the energy location of the features of the Mn XANES spectra of the different Mn species, the energies of these 116 progressive scans were: 6,690 to 6,640 in 10 eV decrements (six energies), 6,636 to 6,580 in 4 eV decrements (15 energies), 6,579 to 6,565 in 1 eV decrements (15 energies), 6,564.5 to 6,530.0 in 0.5 eV decrements (70 energies), and 6,528 to 6,510 in 2 eV decrements (10 energies). For the fluorescence-XANES imaging, the step size was 2 μm in the horizontal direction and 6 μm in the vertical direction, with a stage velocity of 2.0 mm s^{-1}. The total scan time for the 116 scans in the XANES stack was approximately 4 h.

Ten standard compounds were analyzed to allow interpretation of the fluorescence-XANES data. The following solids, after grinding and spreading thinly across the surface of a filter paper, were examined: Mn(IV) as Mn oxide (MnO_2); Mn(III) as Mn oxide (Mn_2O_3) and manganite [MnO(OH)]; Mn(II) plus Mn(III) as hausmannite ($Mn^{2+}Mn^{3+}{}_2O_4$); and Mn(II) as hureaulite [$Mn^{2+}{}_5(PO_3OH)_2(PO_4)_2 0.4H_2O$] and Mn carbonate ($MnCO_3$). Solutions of aqueous $MnSO_4$, Mn(II) L-malate, and Mn(II) citrate were prepared at a final Mn

concentration of 3 mM and 15 mM malate or citrate adjusted to pH 6 using NaOH. A strip of filter paper (approximately 3 mm wide) was immersed for 3 s in each standard solution. All 10 standards were wrapped in polyimide film, placed on a sample holder, and analyzed using fluorescence-XANES imaging.

For the fluorescence-XANES stacks, the GeoPIXE energy association module was used to identify pixels in selected areas where the speciation varied by comparing the concentration ratios between two energies for each pixel. Pixels were excluded where the concentration of Mn was low and indistinguishable from background noise. The XANES spectra were extracted from pixels within the selected areas in the stack series and subsequently background- and baseline-corrected using Athena version 0.9.2 (Ravel and Newville, 2005). As detailed by Kopittke et al. (2014), LCF was performed using Athena, with the combination of standards yielding the lowest residual parameter chosen as the most likely set of components. No differentiation was made between Mn(II) malate and Mn(II) citrate due to the similarity of the XANES spectra.

The appearance of darkened NGTs in sunflower 8 d after imposing the 100 μM led to the hypothesis that high Mn would accumulate in sunflower leaves soon after transfer to high-Mn solution. This was tested using a short period of remaining allocated time on the XFM beamline using μ-XRF analysis of leaves from plants grown at 0.5 and 100 μM Mn for 1 d. Elemental mapping was conducted, and the fluorescence spectra was analyzed using the CSIRO Dynamic Analysis method in GeoPIXE as described above.

Bulk Speciation

A second solution culture experiment was conducted to determine the bulk speciation of Mn in plant tissues using XAS at the Advanced Photon Source. The same plant growth procedures were used as in the previous experiments to obtain root, stem plus petiole, and leaf samples of plants grown at 100 μM Mn. Mean values ($n = 15$) of selected nutrients in solution at the start and end of each week were (μM): 855 Ca, 82 Mg, 220 K, 11 Na, 18 P, 370 S, 5.4 Fe, 0.12 Cu, 0.56 Zn, and 10 B. The concentration of Mn averaged 89 μM ($n = 9$) in the nominal 100 μM Mn treatment solution. Upon excision, plant tissues were immediately frozen in liquid nitrogen and stored for up to 1 h at −20°C before being freeze dried and then ground at ambient temperature. Concentrations of selected nutrients in freeze-dried plant tissues were determined as in the previous experiment. In keeping with the data in Figure 1, 25 mmol Mn kg^{-1} FM in leaves of white lupin was 3 times higher than that in leaves of the other three species (Supplemental Fig. S16). The Mn in stems was lower than that in the leaves, with the highest Mn in white lupin also. Soybean and narrow-leafed lupin had the highest Mn concentration in roots. Concentrations of other nutrients measured were similar to those of plants at 100 μM Mn in the μ-XRF experiment (data not shown).

XAS data were collected in transmission mode at the Materials Research Collaborative Access Team beamline 10-BM, Sector 10, at the Advanced Photon Source of the Argonne National Laboratory (Kropf et al., 2010). The storage ring operated at 7 GeV in top-up mode. A liquid nitrogen-cooled double crystal Si (111) monochromator was used to select the incident photon energies. Calibration was performed by assigning the first derivative inflection point of the absorption K-edge of Mn metal (6,539 eV), and each sample scan was collected simultaneously with a Mn metal foil. The freeze-dried and ground plant samples were formed into 7-mm pellets and mounted between two sections of Kapton tape in a plastic sample holder for analysis. The leaf, stem, and root tissues from the four plant species (12 samples) were analyzed, with each analysis consisting of two replicate scans. The spectra were truncated to 7,100 eV due to the presence of Fe in the plant tissues. Standards were analyzed as solids, with the solutions of Mn(II) malate and Mn(II) citrate first freeze dried and then ground. Scans were energy normalized using the Athena version 0.9.2 software package (Ravel and Newville, 2005). Athena was used for LCF, with the fitting range of −20 to +30 eV relative to the calibration energy. Principal component analysis of the derivative sample spectra was used in the first instance to estimate the number of Mn species contributing to the overall spectra (Webb, 2005).

Organic Ligand Analysis

Plant samples were analyzed using LC-MS to measure bulk tissue concentrations of simple organic acids. Samples of tissues grown in nutrient solutions with 100 μM Mn were prepared as described by Cataldi et al. (2003). Briefly, samples were frozen in liquid nitrogen, freeze dried, and ground at room temperature. MilliQ water (3 mL with specific resistance of 18.2 MΩ cm) was added to 300 mg tissue, shaken, and centrifuged: samples were then filtered to 0.45 μm prior to analysis. Complete separation of all organic acids was achieved using a reversed-phase column (Zorbax Eclipse Plus C18, 100- × 4.6-mm i.d., 3.5 μm) and guard column (12.5- × 4.6-mm i.d., 5 μm) with a mobile phase of aqueous acetic and formic acids (pH of 2.86). The instrument was operated in the negative mode. The injection volume was 10 μL, and the flow rate was 0.7 mL min^{-1} at a temperature of 20°C. An LC-MS single quadrupole method was developed for the simultaneous determination of a mixture of organic acids comprising citrate, malate, oxalate, maleate, and succinate. Separation occurred within 7 min, and tissue results were compared with standard calibration curves. Mainly malate, citrate, and succinate were present in the plant samples, with oxalate and maleate being below the detection limit and succinate averaging only 0.35 ± 0.03 mg kg^{-1} DM.

Supplemental Data

The following supplemental materials are available.

Supplemental Figure S1. Symptoms of Mn toxicity on soybean leaves and effects on plant growth.

Supplemental Figure S2. Sunflower linear glandular trichomes and NGTs, the latter becoming darkened when grown at 100 μM Mn.

Supplemental Figure S3. Effects of Mn in solution on the Ca concentration in plant leaves, stems, and roots.

Supplemental Figure S4. μ-XRF images of Mn, Ca, and Zn in leaves of plants grown at 0.5 μM Mn in solution.

Supplemental Figure S5. Light micrographs and a μ-XRF image of Mn of a soybean leaf grown at 100 μM Mn.

Supplemental Figure S6. Distributions of Ca, Mn, and Zn in part of a leaf of soybean grown at 100 μM Mn.

Supplemental Figure S7. Distributions of Ca, Mn, and Zn in part of a leaf of narrow-leafed lupin grown at 100 μM Mn.

Supplemental Figure S8. μ-XRF image of Mn in sunflower NGTs and the relative Mn concentration along a traverse of an NGT at 100 μM Mn.

Supplemental Figure S9. μ-XRF images of Mn and Ca distributions in leaves of plants grown at 100 μM Mn in solution.

Supplemental Figure S10. μ-XRF image of Mn in plant roots grown at 100 μM Mn in solution.

Supplemental Figure S11. Projected volumetric concentration of Mn in transects of roots grown at 100 μM Mn in solution.

Supplemental Figure S12. μ-XRF images illustrating the distributions of Mn, Ca, and Zn in sunflower NGTs at 0.5 μM Mn and after 1 d at 100 μM Mn.

Supplemental Figure S13. Normalized K-edge XANES spectra of standard Mn compounds.

Supplemental Figure S14. Normalized K-edge XANES spectra of four Mn (II) standard compounds.

Supplemental Figure S15. Illustration of the procedure used to identify the distribution of Mn populations using XANES imaging and the energy association module in GeoPIXE.

Supplemental Figure S16. Concentration of Mn in freeze-dried leaves, stems, and roots of soybean, white lupin, narrow-leafed lupin, and sunflower grown for 13 d at 100 μM Mn.

Supplemental Table S1. Effects of Mn in solution on the DM of soybean, white lupin, narrow-leafed lupin, and sunflower.

Supplemental Table S2. Concentrations of citrate and malate in leaves, stems, and roots of the four plant species.

Supplemental Table S3. Percentage Mn speciation in roots, stems, and leaves of plants grown for 13 d at 100 μM Mn in solution using LCF.

Supplemental Table S4. DM percentage of soybean, white lupin, narrow-leafed lupin, and sunflower tissues.

Supplemental Results S1. μ-XRF analysis of Mn in the Control treatment.

ACKNOWLEDGMENTS

We thank Dr. Allan Pring (South Australian Museum) for supplying the Mn standards used in the XAS study, Cui Li (University of Queensland) for the scanning electron micrographs in Supplemental Figure S2, and Dr. Martin de Jonge (Australian Synchrotron), Dr. Daryl Howard (Australian Synchrotron), and Dr. Chris Ryan (Commonwealth Scientific and Industrial Research Organization) for the XANES imaging technique. The U.S. Environmental Protection Agency (USEPA) contributed to this article but the research was neither performed nor funded by the USEPA and is not subject to the USEPA's quality system requirements. Consequently, the views, interpretations, and conclusions expressed in this article are solely those of the authors and do not necessarily reflect or represent the USEPA's views or policies.

Received May 19, 2015; accepted September 21, 2015; published September 22, 2015.

LITERATURE CITED

Aschenbrenner AK, Horakh S, Spring O (2013) Linear glandular trichomes of *Helianthus* (Asteraceae): morphology, localization, metabolite activity and occurrence. AoB Plants **5:** plt028

Blamey FPC, Joyce DC, Edwards DG, Asher CJ (1986) Role of trichomes in sunflower tolerance to manganese toxicity. Plant Soil **91:** 171–180

Broadhurst CL, Chaney RL, Angle JS, Maugel TK, Erbe EF, Murphy CA (2004) Simultaneous hyperaccumulation of nickel, manganese, and calcium in *Alyssum* leaf trichomes. Environ Sci Technol **38:** 5797–5802

Broadhurst CL, Tappero RV, Maugel TK, Erbe EF, Sparks DL, Chaney RL (2009) Interaction of nickel and manganese in accumulation and localization in leaves of the Ni hyperaccumulators *Alyssum murale* and *Alyssum corsicum*. Plant Soil **314:** 35–48

Cataldi TRI, Margiotta G, Del Fiore A, Bufo SA (2003) Ionic content in plant extracts determined by ion chromatography with conductivity detection. Phytochem Anal **14:** 176–183

Clarkson DT (1988) The uptake and translocation of manganese by plant roots. *In* RD Graham, RJ Hannam, NC Uren, eds, Manganese in Soils and Plants. Kluwer Academic Publishers, Dordrecht, The Netherlands, pp 101–111

Dou CM, Fu XP, Chen XC, Shi JY, Chen YX (2009) Accumulation and interaction of calcium and manganese in *Phytolacca americana*. Plant Sci **177:** 601–606

Edwards DG, Asher CJ (1982) Tolerance of crop and pasture species to manganese toxicity. *In* A Scaife, ed, Proceedings of the 9th International Plant Nutrition Colloquium 1. Commonwealth Agricultural Bureaux, Warwick, United Kingdom, pp 145–151

Elamin OM, Wilcox GE (1986a) Effect of magnesium and manganese nutrition on muskmelon growth and manganese toxicity. J Am Soc Hortic Sci **111:** 582–587

Elamin OM, Wilcox GE (1986b) Effect of magnesium and manganese nutrition on watermelon growth and manganese toxicity. J Am Soc Hortic Sci **111:** 588–593

Fernando DR, Marshall AT, Forster PI, Hoebee SE, Siegele R (2013) Multiple metal accumulation within a manganese-specific genus. Am J Bot **100:** 690–700

Fernando DR, Marshall AT, Gouget B, Carriere M, Collins RN, Woodrow IE, Baker AJ (2008) Novel pattern of foliar metal distribution in a manganese hyperaccumulator. Funct Plant Biol **35:** 193–200

Fernando DR, Mizuno T, Woodrow IE, Baker AJM, Collins RN (2010) Characterization of foliar manganese (Mn) in Mn (hyper)accumulators using x-ray absorption spectroscopy. New Phytol **188:** 1014–1027

Führs H, Hartwig M, Molina LEB, Heintz D, Van Dorsselaer A, Braun HP, Horst WJ (2008) Early manganese-toxicity response in *Vigna unguiculata* L.: a proteomic and transcriptomic study. Proteomics **8:** 149–159

George TS, French AS, Brown LK, Karley AJ, White PJ, Ramsay L, Daniell TJ (2014) Genotypic variation in the ability of landraces and commercial cereal varieties to avoid manganese deficiency in soils with limited manganese availability: Is there a role for root-exuded phytases? Physiol Plant **151:** 243–256

Haydon MJ, Cobbett CS (2007) Transporters of ligands for essential metal ions in plants. New Phytol **174:** 499–506

Horiguchi T (1987) Mechanism of manganese toxicity and tolerance of plants. II. Deposition of oxidized manganese in plant tissues. Soil Sci Plant Nutr **33:** 595–606

Horst WJ, Fecht M, Naumann A, Wissemeier AH, Maier P (1999) Physiology of manganese toxicity and tolerance in *Vigna unguiculata* (L.) Walp. J Plant Nutr Soil Sci **162:** 263–274

Hughes NP, Williams RJP (1988) An introduction to manganese biological chemistry. *In* RD Graham, RJ Hannam, NC Uren, eds, Manganese in Soils and Plants. Kluwer Academic Publishers, Dordrecht, The Netherlands, pp 7–19

Kartusch R (2003) On the mechanism of callose synthesis induction by metal ions in onion epidermal cells. Protoplasma **220:** 219–225

Kopittke PM, de Jonge MD, Wang P, McKenna BA, Lombi E, Paterson DJ, Howard DL, James SA, Spiers KM, Ryan CG, et al (2014) Laterally resolved speciation of arsenic in roots of wheat and rice using fluorescence-XANES imaging. New Phytol **201:** 1251–1262

Kopittke PM, Lombi E, McKenna BA, Wang P, Donner E, Webb RI, Blamey FPC, de Jonge MD, Paterson D, Howard DL, et al (2013) Distribution and speciation of Mn in hydrated roots of cowpea at levels inhibiting root growth. Physiol Plant **147:** 453–464

Kopittke PM, Menzies NW, de Jonge MD, McKenna BA, Donner E, Webb RI, Paterson DJ, Howard DL, Ryan CG, Glover CJ, et al (2011) In situ distribution and speciation of toxic copper, nickel, and zinc in hydrated roots of cowpea. Plant Physiol **156:** 663–673

Kropf AJ, Katsoudas J, Chattopadhyay S, Shibata T, Lang EA, Zyryanov VN, Ravel B, McIvor K, Kemner KM, Scheckel KG, et al (2010) The new MRCAT (Sector 10) Bending magnet beamline at the Advanced Photon Source. AIP Conf Proc **1234:** 299–302

Küpper H, Lombi E, Zhao FJ, Wieshammer G, McGrath SP (2001) Cellular compartmentation of nickel in the hyperaccumulators *Alyssum lesbiacum*, *Alyssum bertolonii* and *Thlaspi goesingense*. J Exp Bot **52:** 2291–2300

Lambers H, Hayes PE, Laliberté E, Oliveira RS, Turner BL (2015) Leaf manganese accumulation and phosphorus-acquisition efficiency. Trends Plant Sci **20:** 83–90

Lindsay WL (1979) Chemical Equilibria in Soils. John Wiley and Sons, New York

Liu J, Shang W, Zhang X, Zhu Y, Yu K (2014) Mn accumulation and tolerance in *Celosia argentea* Linn.: a new Mn-hyperaccumulating plant species. J Hazard Mater **267:** 136–141

McNear DHJ, Küpper JV (2014) Mechanisms of trichome-specific Mn accumulation and toxicity in the Ni hyperaccumulator *Alyssum murale*. Plant Soil **377:** 407–422

Millaleo R, Reyes-Diaz M, Ivanov AG, Mora ML, Alberdi M (2010) Manganese as essential and toxic element for plants: transport, accumulation and resistance mechanisms. Journal of Soil Science and Plant Nutrition **10:** 476–494

Neumann G, Romheld V (2012) Rhizosphere chemistry in relation to plant nutrition. *In* P Marschner, ed, Marschner's Mineral Nutrition of Higher Plants, Ed 3. Academic Press, San Diego, pp 347–368

Page V, Weisskopf L, Feller U (2006) Heavy metals in white lupin: uptake, root-to-shoot transfer and redistribution within the plant. New Phytol **171:** 329–341

Paterson DJ, de Jonge MD, McKinlay WLJ, Starritt A, Kusel M, Ryan CG, Kirkham R, Moorhead G, Siddons DP (2011) The x-ray fluorescence microscopy beamline at the Australian synchrotron. AIP Conf Proc **1365:** 219–222

Peiter E, Montanini B, Gobert A, Pedas P, Husted S, Maathuis FJM, Blaudez D, Chalot M, Sanders D (2007) A secretory pathway-localized cation diffusion facilitator confers plant manganese tolerance. Proc Natl Acad Sci USA **104:** 8532–8537

Ravel B, Newville M (2005) ATHENA, ARTEMIS, HEPHAESTUS: data analysis for x-ray absorption spectroscopy using IFEFFIT. J Synchrotron Radiat **12:** 537–541

Ryan CG (2000) Quantitative trace element imaging using PIXE and the nuclear microprobe. Int J Imaging Syst Technol **11:** 219–230

Ryan CG, Jamieson DN (1993) Dynamic analysis: on-line quantitative PIXE microanalysis and its use in overlap-resolved elemental mapping. Nucl Instrum Methods Phys Res B **77:** 203–214

Stael S, Wurzinger B, Mair A, Mehlmer N, Vothknecht UC, Teige M (2012) Plant organellar calcium signalling: an emerging field. J Exp Bot **63:** 1525–1542

Takahashi M, Terada Y, Nakai I, Nakanishi H, Yoshimura E, Mori S, Nishizawa NK (2003) Role of nicotianamine in the intracellular delivery of metals and plant reproductive development. Plant Cell **15:** 1263–1280

van der Ent A, Baker AJM, Reeves RD, Pollard AJ, Schat H (2013) Hyperaccumulators of metal and metalloid trace elements: facts and fiction. Plant Soil **362:** 319–334

Wang P, Menzies NW, Lombi E, McKenna BA, de Jonge MD, Donner E, Blamey FPC, Ryan CG, Paterson DJ, Howard DL, et al (2013) Quantitative determination of metal and metalloid spatial distribution in hydrated and fresh roots of cowpea using synchrotron-based x-ray fluorescence microscopy. Sci Total Environ **463-464:** 131–139

Webb SM (2005) SIXpack: a graphical user interface for XAS analysis using IFEFFIT. Phys Scr T **115:** 1011–1014

Wissemeier AH, Diening A, Hergenroder A, Horst WJ, Mix-Wagner G (1992) Callose formation as parameter for assessing genotypical plant tolerance of aluminium and manganese. Plant Soil **146:** 67–75

Wissemeier AH, Horst WJ (1992) Effect of light intensity on manganese toxicity symptoms and callose formation in cowpea (*Vigna unguiculata* (L.) Walp.). Plant Soil **143:** 299–309